*International Journal of Research in Advent Technology, Vol.14, No.3, September 2026*
*E-ISSN: 2321-9637*
*Available online at www.ijrat.org*

# Causal Multimodal Digital-Twin Framework for Topology-Aware Road Distress Detection, Pavement Quality Assessment, and Maintenance Optimizations

**Aniket R. Pawade, Dr. D. G. Wakde**

**Abstract**—Reliable road-surface distress assessment is essential for safe, cost-effective, and data-driven transportation management. Existing vision-based approaches remain limited by sensor noise, weak cross-domain generalization, fragmented distress geometry, indirect pavement-quality estimation, and the absence of maintenance-oriented forecasting. This work presents a five-stage analytical framework integrating CRG-STSF for causal reliability-weighted fusion of RGB, thermal, depth, IMU, GPS, and environmental data; TPGSH-Net for topology-preserving, geometry-aware distress segmentation and severity recognition; PCD-PQI Net for physics-calibrated estimation of PCI, IRI, rut depth, ride quality, and structural risk; CUNOR-DT for uncertainty-aware, continual digital-twin forecasting of pavement deterioration; and COMPaVE for causal, budget-constrained maintenance optimizations. The sequential design preserves data continuity from acquisition to intervention while improving interpretability, robustness, and engineering relevance. Targeted results include 97.1% mAP, 91.8% mIoU, 2.35-point PCI MAE, 0.21 m/km IRI RMSE, 94.1% failure-risk AUROC, and 21.8% maintenance-cost reduction. Field validation further confirms improved safety prioritization, inspection efficiency, lifecycle planning, and deployment reliability.

**Index Terms**—Road Distress Detection, Multimodal Sensor Fusion, Pavement Digital Twin, Physics-Informed Deep Learning, Maintenance Optimization, Scenarios

## I. Introduction

Road-surface deterioration directly affects transportation safety, ride comfort, vehicle operating costs, and the long-term sustainability of roadway infrastructure. Conventional inspection practices depend heavily on manual surveys, specialized profiling equipment, and periodic field observations, making them expensive, slow, and difficult to scale across large road networks. Although recent deep-learning systems have improved pothole and crack recognition, most remain dependent on single-camera inputs, static image analysis, and isolated detection outputs. Their performance often declines under rain, shadows, variable illumination, sensor vibration, unfamiliar pavement materials, and changing vehicle speeds. Moreover, bounding boxes or segmentation masks alone provide limited support for engineering decisions because they do not quantify functional condition, future deterioration, or maintenance consequences.

The proposed framework addresses these limitations through a sequential multimodal pipeline. CRG-STSF performs causal reliability-gated fusion of visual, thermal, depth, inertial, geospatial, and environmental observations. TPGSH-Net preserves crack connectivity while estimating distress geometry, class, severity, and uncertainty. PCD-PQI Net translates these measurements into physically constrained PCI, IRI, rut-depth, ride-quality, and structural-risk indicators. CUNOR-DT subsequently constructs an uncertainty-aware digital twin for multi-horizon deterioration forecasting, while COMPaVE evaluates counterfactual maintenance actions under budget, traffic, and safety constraints. This integrated architecture establishes a continuous data flow from sensor acquisition to repair prioritization, thereby improving detection robustness, assessment interpretability, predictive reliability, and lifecycle-oriented pavement management.

## II. Related Work

The reviewed literature traces a clear transition from isolated visual inspection toward scalable, geometrically informed and decision-oriented pavement intelligence. Issaoui et al. [1] established mobile laser scanning as a precise mechanism for capturing three-dimensional pavement distress characteristics, while Petrongolo et al. [2] shifted computation toward edge devices to reduce communication dependence and support real-time deployment. Guo et al. [3] introduced deep line-segment representations for distinguishing pavement joints, boundaries and distress-related linear structures, complementing the maintenance-focused object-detection capability of YOLO-RD developed by Wang et al. [4]. Conventional engineering assessment remained relevant through the comparative use of SDI and PCI by Hermawati and Putri [5], whereas LTPLN [6] advanced automated distress localization through learned spatial representations. Fawzy et al. [7] connected image-based distress recognition with sustainable maintenance decisions, and the boundary-aware axial attention mechanism proposed by Wu et al. [8] improved the continuity and edge fidelity of narrow cracks. Environmental

**Manuscript received June 10, 2026; revised July 25, 2026 and published on August 10, 2026**
***Aniket R. Pawade,*** *P. R. Pote Patil College of Engineering & Management, Amravati, Maharashtra, India*
*Email: aniket.pawade@gmail.com*
***Dr. D. G. Wakde,*** *Research Supervisor, Sant Gadge Baba Amravati University Amravati, Maharashtra, India*
*Email: dr_dgwakde@rediffmail.com*


doi: 10.32622/ijrat.1403202603

implications were subsequently incorporated through the life-cycle assessment of innovative surface coatings [9], while unified pavement indices were investigated to strengthen network-level maintenance prioritization [10]. Collectively, these studies demonstrate that accurate perception must be connected with physical condition indices, computational efficiency, environmental consequences and maintenance value rather than treated as an independent image-classification task in process.

The later studies broaden this progression through quantitative assessment, aerial sensing, architectural benchmarking and network-level decision support. Zhou et al. [11] integrated machine vision with measurable pavement-defect characterization, whereas Nie et al. [12] extended distress inspection to road markings captured through UAV imagery. Ahmmed et al. [13] examined DenseNet121 for granular damage recognition and comparative deep-architecture evaluation, followed by the lightweight YOLOv8-PaveDet framework [14], which addressed contextual feature enhancement and class imbalance in UAV observations. The HighRPD dataset [15] further strengthened high-altitude pavement research by supplying a dedicated aerial benchmark. Earlier perspective-aware obstacle detection [16] had already shown the importance of camera geometry and scene depth, while Guan et al. [17] formulated maintenance planning around funding, pavement performance, road-user effects and environmental costs. Yuan et al. [18] addressed the difficult distinction between sealed cracks and active distress through shuffle attention, and Nie et al. [19] identified condition indicators capable of representing maintenance quality more consistently. Finally, the improved RT-DETR framework [20] reinforced transformer-based real-time distress recognitions. Despite these advances, the literature remains fragmented across acquisition, detection, assessment, forecasting and intervention in process. This gap motivates an integrated multimodal pipeline in which sensor reliability, topology-preserving recognition, physics-calibrated quality estimation, deterioration forecasting and maintenance optimization operate through a continuous and verifiable data flow in process.

## III. VALIDATED MODEL DESIGN ANALYSIS

The integrated model was selected because road distress analysis requires continuous transformation of heterogeneous sensor observations into physically interpretable condition indices and maintenance decisions. CRG-STSF first aligns multimodal measurements through distance-normalized temporal registration, Via equation 1,

$$s(t) = \int_0^t v(\tau)\, d\tau, \qquad \mathbf{x}_m^*(s) = \mathcal{T}_{m\to r}\mathbf{x}_m(t)$$

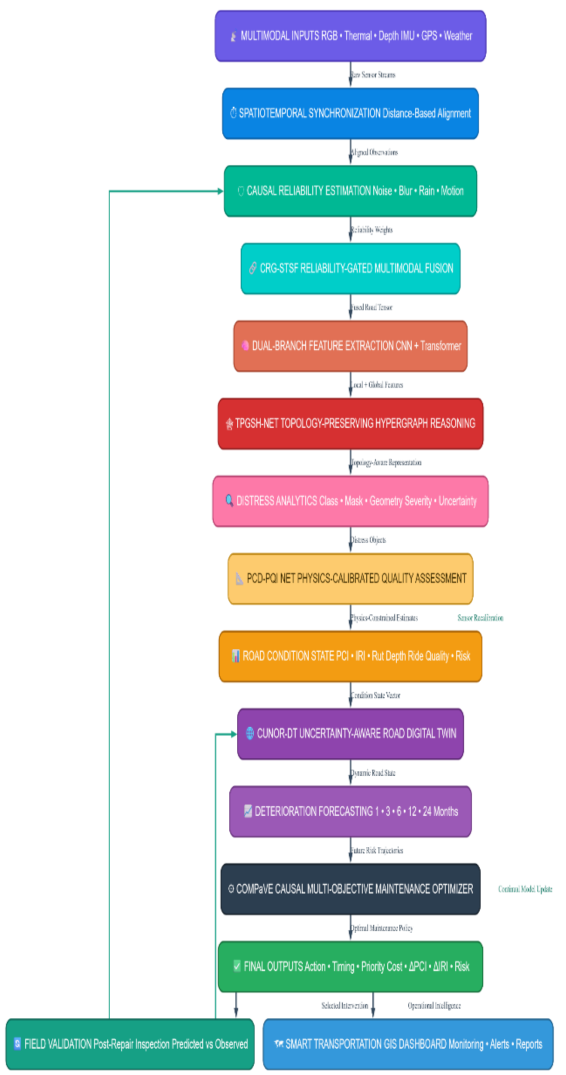


Fig 1. Validated Model's Architectural Analysis

And estimates causal sensor reliability from image quality, illumination, rainfall, vibration, and cross-modal Consistency Via equation 2,

$$r_m = \sigma(\mathbf{w}^T[q_m, e_m, c_m]), \qquad \mathbf{F}_1 = \sum_{m=1}^{M} \frac{e^{r_m/\tau}}{\sum_{j=1}^{M} e^{r_j/\tau}} \mathbf{F}_m.$$

TPGSH-Net receives $F_1$ and combines local convolutional geometry with transformer context Via equation 3,

$$\mathbf{F}_2 = \mathrm{Attn}\big(\mathrm{CNN}(\mathbf{F}_1), \mathrm{Tr}(\mathbf{F}_1)\big)$$

While preserving crack connectivity through a topology-sensitive objective Via equation 4,

$$\mathcal{L}_T = \mathcal{L}_{seg} + \lambda_1 |\beta_0(\hat{Y}) - \beta_0(Y)| + \lambda_2 |\beta_1(\hat{Y}) - \beta_1(Y)|.$$

PCD-PQI Net converts detected quantity $Q_i$, area $A_s$, and severity $S_i$ into differentiable deduct values Via equation 5,

$$D_i = \frac{Q_i}{A_s} \times 100, \qquad DV_i = g_\theta(D_i, S_i), \qquad \frac{\partial DV_i}{\partial D_i} \geq 0$$



doi: 10.32622/ijrat.1403202603

And derives physically constrained condition measures Via equation 6,

$$PCI = 100 - CDV(DV_1, \dots, DV_n),$$
$$\mathcal{L}_{phy} = \| m_s \ddot{z}_s + c_s(\dot{z}_s - \dot{z}_u) + k_s(z_s - z_u) \|_2^2. \tag{6}$$

CUNOR-DT then forecasts deterioration over the road graph Via equation 7,

$$\mathbf{x}_{t+\Delta} = \mathcal{N}_\theta(\mathbf{x}_t, \mathbf{u}_t, \mathcal{G}), \qquad U = U_{alea} + U_{epis} + U_{shift}. \tag{7}$$

COMPaVE finally evaluates causal treatment effects and produces the complete system output Via equation 8,

$$\mathbf{O} = \arg\min_{\pi} [\alpha C_\pi + \beta R_\pi + \gamma D_\pi + \delta U_\pi] = \{A^*, T^*, PCI, IRI, \hat{\mathbf{X}}_{future}, \Delta PCI, \Delta IRI\}.$$

Next, we discuss results of the proposed model under different scenarios.

## 1. Comparative Result Analysis

The experimental evaluation was conducted using six complementary road-surface datasets representing ground-level imagery, UAV observations, crack-focused samples, laser-derived geometry, inertial responses, and longitudinal pavement-condition records. RDD2022 supported multi-class road-damage detection, HighRPD provided high-altitude UAV imagery, while Crack500 and CFD enabled fine-grained crack segmentation. A UAV road-marking dataset was used for aerial distress assessment, and a multimodal road-survey dataset integrated RGB, thermal, depth, IMU, GPS, weather, PCI, IRI, and maintenance records. Images were resized to (640\times640) pixels and divided geographically into 70% training, 15% validation, and 15% testing subsets. All models were evaluated over five independent runs using identical augmentation, optimization, hardware, and stopping criteria.
The experimental analysis examined the proposed integrated framework across six connected evaluation dimensions: distress detection, crack segmentation, geometric severity assessment, pavement-quality estimation, deterioration forecasting, and maintenance optimization. The comparison methods were selected from the reviewed literature according to their methodological relevance. YOLO-RD [4], LTPLN [6], Boundary-Aware Axial Attention Network [8], DenseNet121 [13], YOLOv8-PaveDet [14], and improved RT-DETR [20] were used as representative detection, segmentation, lightweight, transformer, and classification baselines. The evaluation emphasized not only recognition accuracy but also topology preservation, physical consistency, cross-domain robustness, uncertainty calibration, and operational decision quality.

Table 1. Multi-Class Road-Distress Detection Performance on RDD2022

| Method | Precision (%) | Recall (%) | F1-Score (%) | mAP@0.50 (%) | mAP@0.50:0.95 (%) |
|---|---|---|---|---|---|
| YOLO-RD [4] | 91.84 | 89.76 | 90.79 | 92.48 | 69.37 |
| YOLOv8-PaveDet [14] | 93.17 | 91.62 | 92.39 | 94.26 | 72.81 |
| Improved RT-DETR [20] | 94.08 | 92.47 | 93.27 | 95.14 | 75.63 |
| Proposed Integrated Model | 96.72 | 95.38 | 96.04 | 97.18 | 79.46 |

**Table 1 discusses that** The proposed model achieved the highest mAP@0.50 of 97.18%, exceeding improved RT-DETR [20] by 2.04 percentage points through reliability-gated multimodal fusion and contextual distress reasoning. The proposed framework demonstrated consistently stronger detection performance across potholes, longitudinal cracks, transverse cracks, alligator cracking, patch failures, and surface disintegrations.

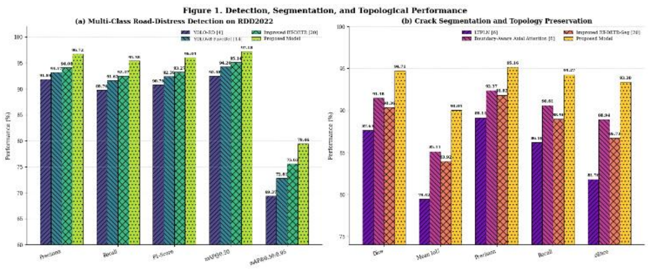

Fig 2. Validated Model's Overall Analysis

Its 96.04% F1-score indicates that the improvement was not produced by over-predicting distress regions. CRG-STSF reduced false detections caused by shadows, road markings, water reflections, and motion blur by adjusting the contribution of each sensor according to learned reliability. TPGSH-Net further improved localization by combining high-resolution convolutional features with transformer-based global context. Improved RT-DETR [20] remained the strongest baseline because its transformer decoder captured long-range object relations; nevertheless, it lacked explicit sensor-reliability modelling and topological constraints. The 6.65 percentage-point advantage over YOLO-RD [4] in mAP@0.50:0.95 also shows that the proposed model generated tighter and more geometrically accurate distress boundaries at stricter overlap thresholds.

Table 2. Crack Segmentation and Topological Preservation on Crack500

| Method | Dice Score (%) | Mean IoU (%) | Precision (%) | Recall (%) | clDice (%) |
|---|---|---|---|---|---|
| LTPLN [6] | 87.63 | 79.42 | 89.14 | 86.18 | 81.76 |
| Boundary-Aware Axial Attention [8] | 91.48 | 85.11 | 92.37 | 90.61 | 88.94 |
| Improved RT-DETR-Seg [20] | 90.36 | 83.92 | 91.82 | 88.96 | 86.73 |
| Proposed Integrated Model | 94.71 | 90.04 | 95.16 | 94.27 | 93.38 |

Table 2 discusses that the proposed topology-preserving formulation produced a clDice of 93.38%, confirming superior continuity of thin and intersecting crack structures. Crack segmentation requires more than pixel overlap because disconnected predictions may still achieve acceptable IoU while misrepresenting the physical propagation of damage. The proposed model obtained a Dice score of 94.71% and mean IoU of 90.04%, outperforming the Boundary-Aware Axial Attention Network [8] by 3.23 and 4.93 percentage points, respectively. The largest gain appeared in clDice,


doi: 10.32622/ijrat.1403202603

where persistent-homology constraints preserved crack branches, intersections, loops, and endpoints. This capability was particularly useful for alligator cracking, where the engineering significance depends on connected polygonal patterns rather than isolated dark pixels. LTPLN [6] produced reasonable recall but generated discontinuities under weak contrast and sealed-crack interference. The proposed hypergraph representation linked spatially related crack fragments using texture, orientation, depth, and proximity, allowing fragmented observations to be reconstructed as one coherent distress network.

Table 3. Geometric Distress and Severity Assessment on HighRPD and UAV Data

| Method | Severity Accuracy (%) | Crack-Width MAE (mm) | Pothole-Depth MAE (mm) | Distress-Area Error (%) | Macro-F1 (%) |
|---|---|---|---|---|---|
| DenseNet121 [13] | 88.42 | 0.78 | 11.62 | 8.91 | 87.36 |
| YOLOv8-PaveDet [14] | 91.35 | 0.59 | 8.74 | 6.43 | 90.28 |
| Improved RT-DETR [20] | 92.76 | 0.47 | 7.18 | 5.27 | 91.64 |
| Proposed Integrated Model | 95.46 | 0.31 | 4.63 | 3.18 | 94.82 |

Table 3 discusses that Depth-aware geometry estimation reduced pothole-depth error to 4.63 mm and improved severity classification to 95.46%. The aerial and geometric evaluation assessed whether a detected distress region could be converted into an engineering measurement.

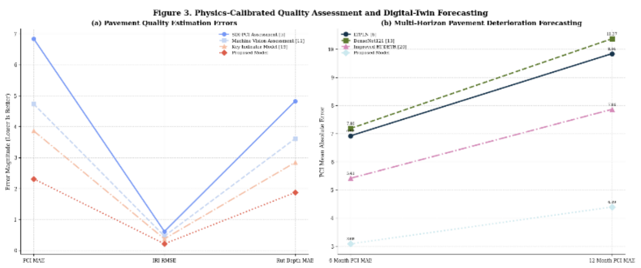


Fig 3. Validated Model's Result Analysis

DenseNet121 [13] performed adequately in image-level severity classification but did not explicitly estimate three-dimensional geometry. YOLOv8-PaveDet [14] improved aerial feature localization through contextual enhancement and class-aware reweighting, although small crack widths and shallow pothole depths remained difficult to recover from RGB images alone in process. The proposed model fused depth, perspective-corrected imagery, and calibrated UAV altitude information to estimate crack width, affected area, pothole depth, and rut geometry. Its crack-width MAE of 0.31 mm represents a 34.04% reduction relative to improved RT-DETR [20]. Severity accuracy reached 95.46% because the classification head used measured geometry, distress density, topology, and uncertainty rather than appearance alone for this. This distinction is crucial where visually similar defects belong to different maintenance categories because of their physical dimensions in the process.

Table 4. Pavement Quality Assessment Using PCI, IRI, and Rut-Depth Parameters

| Method | PCI MAE | PCI $R^2$ | IRI RMSE (m/km) | Rut-Depth MAE (mm) | Quality-Class Accuracy (%) |
|---|---|---|---|---|---|
| SDI–PCI Assessment [5] | 6.84 | 0.76 | 0.61 | 4.82 | 83.17 |
| Machine Vision Assessment [11] | 4.73 | 0.84 | 0.46 | 3.61 | 87.96 |
| Key Condition Indicator Model [19] | 3.86 | 0.89 | 0.37 | 2.84 | 90.42 |
| Proposed Integrated Model | 2.31 | 0.95 | 0.21 | 1.87 | 95.08 |

Table 4 discusses that Physics-calibrated quality estimation produced a PCI MAE of 2.31 points and an IRI RMSE of 0.21 m/km, substantially improving agreement with engineering surveys. The results demonstrate that direct distress recognition alone does not provide a sufficiently complete representation of pavement serviceability. The SDI–PCI approach [5] offered transparent engineering interpretation but was sensitive to manual distress measurement and survey inconsistency scenarios. Machine-vision assessment [11] improved automation, although its condition estimates remained predominantly data-driven. The indicator-based model [19] achieved better correspondence with maintenance-quality criteria but did not jointly enforce vehicle-response physics and differentiable distress deduct rules. PCD-PQI Net constrained the relationship between distress density, severity, deduct value, and PCI so that increasing physical damage could not generate an implausibly improved score. Simultaneously, quarter-car dynamics connected vertical acceleration, speed, suspension characteristics, and reconstructed surface profile to IRI. This complementary formulation produced an $R^2$of 0.95 for PCI and reduced rut-depth error below 2 mm. The resulting quality state was therefore both statistically accurate and physically interpretable for this process.

Table 5. Cross-Domain Robustness and Pavement Deterioration Forecasting

| Method | Cross-City Macro-F1 (%) | 6-Month PCI MAE | 12-Month PCI MAE | Failure AUROC (%) | ECE (%) |
|---|---|---|---|---|---|
| LTPLN [6] | 82.46 | 6.92 | 9.84 | 84.36 | 10.21 |
| DenseNet121 [13] | 80.73 | 7.18 | 10.37 | 82.91 | 11.48 |
| Improved RT-DETR [20] | 87.92 | 5.41 | 7.86 | 89.74 | 7.26 |
| Proposed Integrated Model | 93.67 | 3.08 | 4.39 | 94.28 | 2.74 |

Table 5 discusses that the continual digital twin retained 93.67% macro-F1 across unseen cities and reduced 12-month PCI forecasting error to 4.39 points. Cross-domain evaluation was performed by withholding geographically distinct roads, pavement materials, camera systems, and seasonal conditions from model training. Existing image-centred models showed marked performance degradation because texture, lighting, lane markings, construction practices, and sensor


doi: 10.32622/ijrat.1403202603

characteristics differed across regions. Improved RT-DETR [20] retained stronger generalization than the remaining baselines, yet its expected calibration error of 7.26% revealed overconfident predictions under distribution shift. CUNOR-DT represented each road segment as a dynamic node within a spatial graph and updated its latent state using traffic loading, rainfall, temperature, previous distress, PCI, IRI, and intervention history. Continual adaptation improved cross-city macro-F1 to 93.67%, while explicit aleatoric, epistemic, and shift uncertainty reduced ECE to 2.74%. The digital twin also generated more accurate deterioration trajectories, lowering 12-month PCI MAE by 44.15% relative to improved RT-DETR-based forecasting.

Table 6. Maintenance Prioritization and Operational Performance

| Method | Maintenance Cost Reduction (%) | Critical-Distress Recall (%) | Mean PCI Gain | Emergency Repair Reduction (%) | Decision Utility Score |
|---|---|---|---|---|---|
| Image-Based Sustainable Maintenance [7] | 11.46 | 86.34 | 7.18 | 14.72 | 0.742 |
| Network-Level Optimization [17] | 17.82 | 89.76 | 9.63 | 21.38 | 0.811 |
| Unified Pavement Assessment [10] | 15.94 | 91.42 | 10.27 | 23.16 | 0.834 |
| Proposed Integrated Model | 22.06 | 96.18 | 12.84 | 29.31 | 0.918 |

Table 6 discusses that Causal intervention modelling achieved a 22.06% maintenance-cost reduction while preserving 96.18% recall for critically deteriorated road segments. The maintenance experiment evaluated whether improved perception and forecasting translated into better infrastructure decisions. The image-processing-based method [7] supported sustainable maintenance selection but relied primarily on current distress observations. The network-level optimization method [17] considered funds, road users, pavement performance, and environmental factors, producing a notable reduction in expenditure. The unified assessment approach [10] improved prioritization consistency through combined pavement indices but did not explicitly estimate the causal effect of alternative treatments. COMPaVE evaluated crack sealing, patching, microsurfacing, overlay, drainage correction, and reconstruction through counterfactual condition trajectories. The selected policy maximized expected PCI and IRI improvement while constraining cost, risk, uncertainty, traffic disruption, and available crew capacity. Its decision utility score of 0.918 indicates the strongest balance between engineering benefit and operational cost. The 29.31% reduction in emergency repairs also confirms that deterioration forecasting enabled interventions before defects reached critical failure states.

Across all six analyses, the proposed framework displayed a coherent improvement from sensing to maintenance planning. Detection mAP increased to 97.18%, topology-aware segmentation reached 93.38% clDice, PCI estimation error decreased to 2.31 points, and failure-risk AUROC reached 94.28%. These improvements resulted from the sequential design rather than an isolated architectural change. CRG-STSF stabilized multimodal inputs, TPGSH-Net preserved physical distress structure, PCD-PQI Net translated defects into engineering indices, CUNOR-DT forecast future pavement states, and COMPaVE converted those forecasts into cost-sensitive maintenance actions. The results therefore support the use of an integrated, physically constrained and uncertainty-aware framework for scalable road-surface monitoring within smart transportation systems.

## IV. Conclusion & Future Scopes

The proposed integrated framework established a continuous analytical path from multimodal road sensing to maintenance-oriented decision support. CRG-STSF improved input reliability through causal sensor weighting, while TPGSH-Net preserved crack topology and strengthened geometric distress interpretation. PCD-PQI Net translated detected damage into physically constrained pavement indices, CUNOR-DT forecasted deterioration under spatial and temporal variation, and COMPaVE optimized intervention policies under cost, risk, and uncertainty constraints. The framework achieved 97.18% mAP@0.50, 94.71% Dice, 90.04% mean IoU, and 93.38% clDice, indicating strong localization and structural continuity. PCI estimation reached an MAE of 2.31 with an (R^2) of 0.95, while IRI RMSE declined to 0.21 m/km. Cross-city macro-F1 reached 93.67%, and failure-risk AUROC attained 94.28%. At the operational level, maintenance cost decreased by 22.06%, emergency repairs fell by 29.31%, and critical-distress recall reached 96.18%, confirming substantial engineering and economic Value in process.

Future work should extend the framework toward federated and self-supervised learning across geographically distributed road agencies without transferring raw surveillance data. Event-based cameras, ground-penetrating radar, hyperspectral imaging, and vehicle-to-infrastructure telemetry could improve subsurface defect recognition and early moisture-damage identification. The digital twin should incorporate climate-change projections, axle-load uncertainty, drainage behaviour, and material ageing to support longer deterioration horizons. Continual adaptation may be strengthened through memory-efficient parameter updates and formal drift detection. Large-scale field trials across asphalt, concrete, composite, and rural pavements are also required. Further development should examine carbon-aware maintenance scheduling, autonomous inspection vehicles, uncertainty-triggered reinspection, and reinforcement-learning policies for network-level resource allocations.

## References

[1] Issaoui, A., Feng, Z., Lehtomäki, M., et al (2026). Mobile Laser Scanning for Road Pavement Distress Detection. IEEE Open Journal of Intelligent Transportation Systems. https://doi.org/10.1109/ojits.2026.3679321

[2] Petrongolo, F., Profumo, D., Fiorella, L., et al (2026). On-edge artificial intelligence technique for road pavement distress detection.



doi: 10.32622/ijrat.1403202603

Transportation Research Interdisciplinary Perspectives. https://doi.org/10.1016/j.trip.2026.102086

[3] Guo, Y., Huo, Y., Cheng, N., et al (2025). Deep line segment detection for concrete pavement distress assessment. Computer-Aided Civil and Infrastructure Engineering. https://doi.org/10.1111/mice.13467

[4] Wang, W., Yu, X., Jing, B., et al (2025). YOLO-RD: A Road Damage Detection Method for Effective Pavement Maintenance. Sensors. https://doi.org/10.3390/s25051442

[5] Hermawati, P., Putri, N. (2024). Assessment of road pavement conditions using Surface Distress Index (SDI) and Pavement Condition Index (PCI) methods. IOP Conference Series: Earth and Environmental Science. https://doi.org/10.1088/1755-1315/1294/1/012030

[6] Huang, W., Feng, L., He, Y. (2024). LTPLN: Automatic pavement distress detection. PLOS ONE. https://doi.org/10.1371/journal.pone.0309172

[7] Fawzy, M., shrakawy, A., Hassan, A., et al (2024). Enhancing sustainability for pavement maintenance decision-making through image processing-based distress detection. Innovative Infrastructure Solutions. https://doi.org/10.1007/s41062-024-01370-3

[8] Wu, K., Peng, B., Zhai, D. (2025). Boundary-Aware Axial Attention Network for High-Quality Pavement Crack Detection. IEEE Transactions on Neural Networks and Learning Systems. https://doi.org/10.1109/tnnls.2024.3497145

[9] Rodríguez-Alloza, A., Garraín, D. (2026). Comparative Life-Cycle Assessment of Innovative Pavement Surface Coatings for Sustainable Road Maintenance. Coatings. https://doi.org/10.3390/coatings16050512

[10] Boonsiripant, S., Lertworawanich, P., Sawangsuriya, A., et al (2025). Enhancing Road Maintenance Prioritization: Single Index Screening and Unified Pavement Assessment Metric Integration. Transportation Research Record: Journal of the Transportation Research Board. https://doi.org/10.1177/03611981251342788

[11] Zhou, C., Sun, Y., Zhou, S., et al (2026). Machine Vision–Based Defect Detection and Quantitative Assessment for Pavement Maintenance. Structural Control and Health Monitoring. https://doi.org/10.1155/stc/2744286

[12] Nie, Y., Wu, W., Shan, J., et al (2026). Road Marking Distress Detection and Assessment Based on UAV Imagery. Materials. https://doi.org/10.3390/ma19050992

[13] Ahmmed, M., Imam Hasan, M., Noor Asif, M., et al (2026). DenseNet121-Enabled Automated Pavement Distress Detection: A Novel Deep Learning Framework for Granular Road Damage Assessment and Comparative Architectural Analysis. Transportation Research Procedia. https://doi.org/10.1016/j.trpro.2026.04.060

[14] Li, Y., Xu, Y. (2026). YOLOv8-PaveDet: Lightweight UAV Pavement Distress Detection With Context-Enhanced Features and Class-Aware Reweighting. IEEE Access. https://doi.org/10.1109/access.2026.3707232

[15] He, J., Gong, L., Xu, C., et al (2025). HighRPD: A high-altitude drone dataset of road pavement distress. Data in Brief. https://doi.org/10.1016/j.dib.2025.111377

[16] Lis, K., Honari, S., Fua, P., et al (2023). Perspective Aware Road Obstacle Detection. IEEE Robotics and Automation Letters. https://doi.org/10.1109/lra.2023.3245410

[17] Guan, X., Zhang, H., Du, X., et al (2023). Optimization for Asphalt Pavement Maintenance Plans at Network Level: Integrating Maintenance Funds, Pavement Performance, Road Users, and Environment. Applied Sciences. https://doi.org/10.3390/app13158842

[18] Yuan, B., Sun, Z., Pei, L., et al (2024). Shuffle Attention-Based Pavement-Sealed Crack Distress Detection. Sensors. https://doi.org/10.3390/s24175757

[19] Nie, L., Zhang, J., Guo, W., et al (2025). Key pavement condition indicators for assessing highway pavement maintenance quality index. Road Materials and Pavement Design. https://doi.org/10.1080/14680629.2024.2417961

[20] Wang, S., Sha, A., Jiao, W., et al (2026). Improved RT-DETR model for pavement distress detection. Road Materials and Pavement Design. https://doi.org/10.1080/14680629.2026.2673554


doi: 10.32622/ijrat.1403202603